Available online at www.sciencedirect.com
ScienceDirect
Ceramics International 35 (2009) 3081–3090
CERAMICS INTERNATIONAL
www.elsevier.com/locate/ceramint

Thermodynamic evaluation of the Al_2O_3–H_2O binary system at pressures up to 30 MPa

S. Serena [a,*], M.A. Raso [b], M.A. Rodríguez [a], A. Caballero [a], T.J. Leo [c]

[a] *Instituto de Cerámica y Vidrio (CSIC), C/Kelsen n° 5. Campus de Cantoblanco, 28049 Madrid, Spain*
[b] *Fac. Ciencias Químicas, Universidad Complutense de Madrid (UCM), Ciudad Universitaria, 28040 Madrid, Spain*
[c] *Escuela Técnica Superior de Ingenieros Aeronáuticos, Universidad Politécnica de Madrid (UPM), Pza. Cardenal Cisneros 3, Ciudad Universitaria, 28040 Madrid, Spain*

Received 17 October 2008; received in revised form 9 March 2009; accepted 17 April 2009
Available online 21 May 2009

Abstract

The behaviour of the hydrated phases in the Al_2O_3–H_2O system is of major importance in the chemistry of ceramic materials. In this work, stability and metastability relations in the Al_2O_3–H_2O system have been studied. Gibbs free energy functions of the gibbsite and boehmite phases have been critically revised and new optimized functions have been calculated. The functions obtained have been used to predict the stability and metastability relations by calculating a *P–T* diagram following the CALPHAD methodology. Comparison with the corresponding available experimental data is discussed.

Keywords: Thermodynamic assessment; Al_2O_3–H_2O; Gibbsite; Boehmite

1. Introduction

Aluminium hydroxides are used as the starting material for the manufacturing of transition aluminas, materials widely used for catalysts, coatings and ceramics preparation. Synthetic routes involve the decomposition of aluminium hydroxides, which explains the interest in its dehydration process, thermal stability and reaction kinetics. These phases have important application by themselves; as an example, gibbsite ($Al_2O_3{\cdot}3H_2O$), is an excellent adsorbent for heavy metals [1,2]; boehmite ($Al_2O_3{\cdot}H_2O$) and its dehydrated alumina form are extensively used for preparation of various optical, electronic devices and catalysts [3–5].

The stability of gibbsite and bayerite ($Al_2O_3{\cdot}3H_2O$), boehmite and diaspore ($Al_2O_3{\cdot}H_2O$) phases is a controversial point. Some authors claim the stability of diaspore respect to boehmite and gibbsite even at low pressure [6–8]. According to them, boehmite and gibbsite are just metastable phases appearing as precursors of the diaspore formation. The sluggish kinetics of the transformation of boehmite to diaspore justifies the observation of boehmite at usual experimental conditions or not so long times treatments. The Gibbs free energy functions of boehmite and diaspore are very close but a previous seeding is necessary to obtain diaspore phase. The last means that the activation energy of formation of diaspore is really relevant. Studies on the diaspore–corundum equilibrium [9] are also reported at pressures from 20 MPa up to 200 MPa but the stability relations at high pressures are beyond the scope of the present work.

Gibbsite and boehmite are abundant in nature and they are used as raw materials, so that a detailed knowledge of their hydration/dehydration behaviour is of fundamental importance in the chemistry of ceramic materials, apart from their stability in relation to diaspore. In fact, numerous experimental and theoretical studies on the hydration/dehydration process in boehmite and gibbsite phases can be found in the ceramic literature. However, these studies put in evidence that the process is very sensitive to both environmental conditions and sample processing, so that the stability ranges of the hydrated phases is under discussion nowadays.

The aim of this work is to study, from a thermodynamic point of view, the relative stability of aluminium hydroxide

* Corresponding author. Tel.: +34 91 7355840; fax: +34 91 7355843.
E-mail address: serena@icv.csic.es (S. Serena).

0272-8842/$36.00
doi:10.1016/j.ceramint.2009.04.014

Table 1
Description of the phases in the system Al_2O_3–H_2O, at 25 °C and 1.013×10^5 Pa.

Phase	Crystalline structure	Molar volume, v_0 (m^3/mol)	Thermal expansion, α (K^{-1})	Isothermal compressibility, κ_T (Pa^{-1})
Liquid water H_2O	–	18.052×10^{-6} [10]	2.56×10^{-4} [11]	4.524×10^{-10} [11]
Gas water H_2O	–	–	–	–
Gibbsite $Al_2O_3{\cdot}3H_2O$	Monoclinic $P2_1/n$	32.2328×10^{-6} [10]	42×10^{-6} [12]	2.04×10^{-11} [13]
Boehmite $Al_2O_3{\cdot}H_2O$	Orthorhombic $Cmcm$	19.5401×10^{-6} [10]	32.2×10^{-6} [14]	9.43×10^{-14} [15]
α-Alumina Al_2O_3	Trigonal $R\bar{3}c$	25.813×10^{-6} [10]	26.8×10^{-6} [16]	2.63×10^{-13} [14]

phases in the system Al_2O_3–H_2O in order to predict the corresponding P–T diagram at low pressures (<10 MPa). For this purpose, an extensive revision of the available thermodynamic data has been undertaken and from these data, a set of optimized Gibbs free energy functions have been calculated for gibbsite and boehmite phases, which have been used to obtain the corresponding equilibrium P–T diagram. On the other hand, it is well know that, apart from corundum, the Al_2O_3 composition can be found in different metastable polymorphic forms (γ-, δ-, κ- and χ-Al_2O_3), widely described in the ceramic literature and, consequently, the described decomposition paths are numerous. In this sense, metastability relations using metastable forms for Al_2O_3 have been calculated as well. Finally, a comparison of thermodynamic results with the experimental data is performed.

2. Literature survey

Besides H_2O, within the Al_2O_3–H_2O system the following hydrated compounds appear as stable phases as a function of temperature and pressure: gibbsite (monoclinic $Al_2O_3{\cdot}3H_2O$), bohemite (orthorhombic $Al_2O_3{\cdot}H_2O$), diaspore (orthorhombic $Al_2O_3{\cdot}H_2O$). A brief crystallographic description of the mentioned phases can be found in Table 1 [10–16]. Other metastable polymorphic forms have been also observed for the hydrated phases in the system such as bayerite (hexagonal $Al_2O_3{\cdot}3H_2O$) [17,18]. The Al_2O_3 composition (trigonal α-Al_2O_3, corundum, is the stable phase) [19,20] can be found in different metastable polymorphic forms widely described in the ceramic literature [21,22].

Available experimental data of this system cover: solubility and hydration–dehydration processes, thermodynamic data of the above described compounds and phase equilibrium diagrams. Numerous solubility data have been also published, but this question is out of the scope of this paper. A revision of the hydration–dehydration process proposed in the literature as well as a detailed review of thermodynamic data is presented above.

2.1. Dehydration process in the system

For many years a great number of investigations on the thermal decomposition of aluminium hydroxides have been published, and a sample of relevant and recent papers about this topic is presented in references [11,23–28]. Despite the different experimental methods employed, the dehydration processes nowadays accepted can be described as represented in Fig. 1 [20,29]. Route A is preferred in low grain-size particles or low crystallinity systems, while route B is favoured by high grain-size or high crystallinity particles under conditions of humidity and/or alkalinity. The phase evolution and kinetics of aluminium hydroxide dehydration consequently depends on heating rates, particle size, and atmospheric conditions (e.g., water vapor pressure), and the sequence of metastable polymorphs of Al_2O_3 formed during thermal decompositions is under discussion nowadays [28,11,30].

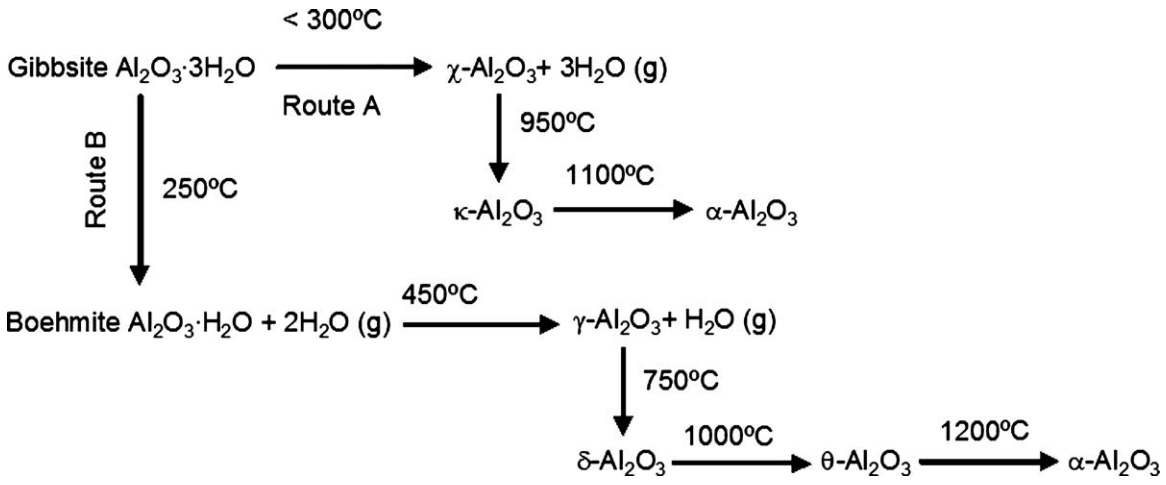

Fig. 1. Typical dehydration sequence of alumina hydrates in air. Starting transition temperatures of the different process are indicated in the figure.

Table 2
Standard Gibbs free energy of formation ($\Delta_f g^\circ_{298.16}$ (kJ/mol)) of aluminium hydroxide phases collected from literature and average value ($\langle\Delta_f g^\circ_{298.16}$ (kJ/mol)$\rangle$).

Gibbsite ($Al_2O_3{\cdot}3H_2O$)	Boehmite ($Al_2O_3{\cdot}H_2O$)	Diaspore ($Al_2O_3{\cdot}H_2O$)
$\Delta_f g^\circ_{298.16}$ (kJ/mol)		
−2320.6 [31]	−1825.4 [32]	−1835.2 ± 3.4 [52]
−2287.4 [32]	−1830 ± 1.6 [49]	−1836 ± 4.2 [49]
−2288.6 ± 2.6 [33]	−1823.7 [36]	−1841.4 ± 3.4 [53]
−2311.2 [34]	−1836.8 ± 4.2 [49]	−1839.2 [36]
−2318.2 [36]	−1828.4 [50]	−1827.56 [38]
−2309.78 [37]	1836.8 ± 4.2 [39]	−1844.0 ± 10.0 [48]
−2310.96 [38]	−1830.6 [41]	−1842.6 [43]
−2309.778 ± 2.426 [39]	−1832.3 [45]	−1841.6 [43]
−2299.17 to 2301.26 [40]	−1842 ± 3 [46]	−1825.4 [45]
−2307.96 [41]	−1833 [51]	
−2315.44 ± 2.84 [43]	−1830.0 ± 3.66 [47]	
−2309 [42]	−1841.28 ± 2.82 [47]	
−2308.28 [44,45]		
−2313.4 ± 3.2 [46]		
−2310.12 ± 2.86 [47]		
$\langle\Delta_f g^\circ_{298.16}$ (kJ/mol)$\rangle$		
−2308.04	−1832.54	−1836.54

Table 3
Standard enthalpy of formation ($\Delta_f h^\circ_{298.16}$ (kJ/mol)) of aluminium hydroxide phases collected from literature.

Gibbsite ($Al_2O_3{\cdot}3H_2O$)	Boehmite ($Al_2O_3{\cdot}H_2O$)	Diaspore ($Al_2O_3{\cdot}H_2O$)
$\Delta_f h^\circ_{298.16}$ (kJ/mol)		
−2563.78 ± 2.52 [54]	−1972.1 ± 16.4 [58]	−2000.60 [59]
−2588.36 ± 5.86 [55]	−1990.68 ± 2.6 [59]	
−2589.8 ± 2.4 [56]	−1991.54 ± 4.0 [60]	
−2586.36 ± 2.4 [57]	−1992.2 ± 2.6 [57]	
$\langle\Delta_f g^\circ_{298.16}$ (kJ/mol)$\rangle$		
−2582.08	−1986.64	−2000.60

Table 4
Entropy values for aluminium hydroxide phases collected from literature.

Gibbsite ($Al_2O_3{\cdot}3H_2O$)	Boehmite ($Al_2O_3{\cdot}H_2O$)	Diaspore ($Al_2O_3{\cdot}H_2O$)
s°_{298} (J/mol K)		
140.07 [67]	96.767 [67]	70.47 [67]
136.77 ± 0.25 [39]	74.32 ± 0.17 [65]	70.61 ± 0.17 [66]
136.9 [10]	96.767 [36]	
140.07 [36]	96.860 [10]	
134.22 ± 0.4 [61]	96.767 ± 0.4 [61]	
$\langle s^\circ_{298}$ (J/mol K)$\rangle$		
136.99	89.32	70.54
Δs°_{298} (J/mol K)		
−923.296 [62]	−500.464 [62]	−526.824 [62]

2.2. Thermodynamic data

Standard Gibbs free energy of formation, standard enthalpy of formation, entropy and constant pressure thermal capacity data of aluminium hydroxide phases found in the literature [31–35] and thermodynamic data bases [10,69] are shown in Tables 2–5. In Table 2 the different standard Gibbs free energy of formation are compared. Standard enthalpies of formation of gibbsite, bayerite, boehmite and diaspore are collected in Table 3. Entropy values at the standard state at 25 °C, s^0_{298} and Δs^0_{298} of aluminium hydroxides are shown in Table 4. Various expressions of the molar thermal capacity as a function of temperature at constant pressure, resulting from experimental data fittings, are given in Table 5 for aluminium hydroxides.

2.3. Phase diagram data

Experimental data on the system Al_2O_3–H_2O can be found in the literature since 1930; most investigations were based on dehydration studies, so that, the values reported for a given transition point may vary up to two hundred degrees, and the equilibrium condition was not always established. A revision of the more systematic studies on this phase diagram is presented in what follows.

The system Al_2O_3–H_2O was studied in 1943 by Laubengayer and Weisz [70] in hydrothermal conditions. The results of the study were presented as a temperature–solubility diagram in which phase stability fields for all mentioned compounds, except for bayerite, were included. According to this diagram, estimated solubility in water follow the sequence gibbsite < boehmite < diaspore < corundum. The stability ranges established in this work for the different phases were: gibbsite

Table 5
Heat capacity data fitting for the aluminium hydroxide phases collected from literature.

Compound	C°_p(J/mol K)	T (K)
Gibbsite ($Al_2O_3{\cdot}3H_2O$)	Experimental (heat content at $T > 298.16$)	<423 [61]
	Experimental measurement	<500 [37]
	$72.314 + 0.38158T$	[62]
	$72.314 + 0.38158T$	298–425 [63]
	$114.7828 + 34.022T - 2.44112 \times 10^5 T^{-2}$	<600 [64]
Boehmite ($Al_2O_3{\cdot}H_2O$)	Experimental (heat content at $T > 298.16$)	<520 [61]
	Experimental measurement	<700 [65]
	$120.792 + 3.514 \times 10^{-2}T$	[62]
	$120.792 + 3.514 \times 10^{-2}T$	298–520 [63]
	$100.3367 + 2.02397 \times 10^{-2}T - 2.69861 \times 10^5 T^{-2}$	<900 [64]
Diaspore ($Al_2O_3{\cdot}H_2O$)	$102.6023 + 0.1093T - 2.42691 \times 10^5 T^{-2}$	<900 [64]
	$94.9696 + 03.5112 \times 10^{-2}T$	[68]

stable up to 155 °C, boehmite apparently stable between 155 °C and 280 °C, diaspore between 280 °C and 450 °C, and corundum stable from 450 °C up.

The behaviour of aluminium under hydrothermal conditions was studied in 1973 by MacDonald and Butler [36] at temperatures between 25 °C and 300 °C. The results from thermodynamic calculation were presented as a series of potential–pH diagrams at various temperatures, and were applied to aluminium corrosion problems.

Ervin and Osborn [19] studied the system Al_2O_3–H_2O at higher temperatures and pressures. Results were expressed as a pressure–temperature diagram, showing stability regions for the crystalline phases, gibbsite, boehmite, diaspore and corundum. The stability field for gibbsite suggested by the authors is located at temperatures lower than 130 °C. At pressures lower than ~6900 MPa the stability region for boehmite was limited by gibbsite (at temperatures lower than 130 °C) and corundum (at temperatures higher that 380 °C). The stability field for diaspore was located at higher pressures between the boehmite and corundum regions, so that an invariant point for the coexistence of boehmite, diaspore, corundum and water appears at 385 ± 15 °C and 13.8 MPa.

Phase relations of the system at high pressures were revised in 1959 by Kennedy [6] who confirmed part of the work of Ervin and Osborn [19] but modified the interpretation of the boehmite–diaspore relationship. These authors explain that the transition diaspore–corundum is reversible, so that real equilibrium conditions can be actually reached. On the contrary, the gibbsite–boehmite transition and boehmite–diaspore transitions are both exceedingly sluggish, so that it is possible that the previous works [19,70] and their own results do not represent equilibrium determinations.

Phase relations in the system at pressures up to 6000 MPa were revisited by Dachille and Gigl [71]. These authors point out to the existence of two new polymorphs of $Al_2O_3{\cdot}3H_2O$, and include their stability field in the *P–T* diagram of the system at pressures higher than 15 kbar (1500 MPa).

3. Thermodynamic models and optimization procedure

Collected experimental information has been used to calculate a group of optimized Gibbs free energy functions of the phases in the system Al_2O_3–H_2O, using the models described below. In the present work, the gaseous mixture phase of the system has been described as an ideal gas. This implies that the *P–V–T* relations and thermodynamic properties of pure gaseous species are calculated as those of an ideal gas so that there is no interaction between gaseous species in the mixture. The solid and liquid phases have been treated as pure phases.

In standard thermodynamic calculations pressure variation of Gibbs energy is usually neglected for non-fluid phases. In this work, the dependence of Gibbs free energy on both temperature and pressure has been taken into account. The expressions of molar Gibbs energy (g) for solid and liquid phases has been calculated from the next equations

$$\begin{aligned} &g = g(T,P)\\ &dg = -s\,dT + v\,dP\\ &v = \left(\frac{\partial g}{\partial P}\right)_T; \quad s = -\left(\frac{\partial g}{\partial T}\right)_P \end{aligned} \tag{1}$$

$$\begin{aligned} dv = \alpha v\,dT - \kappa_T v\,dP \Rightarrow \frac{dv}{v} = \alpha\,dT - \kappa_T\,dP \Rightarrow \ln\left[\frac{v}{v(T^\circ,P^\circ)}\right]\\ = \int_{T^\circ}^{T} \alpha\,dT - \int_{P^\circ}^{P} \kappa_T\,dT, \end{aligned} \tag{2}$$

where v (cm^3/mol) is the molar volume, α is the thermal expansion coefficient (K^{-1}) and κ_T (Pa^{-1}) the isothermal compressibility factor. T° and P° are the usual reference temperature and pressure, 298.15 K and 1.00 bar, respectively. Considering α and κ_T as constants,

$$\begin{aligned} &\ln\left[\frac{v}{v(T^\circ,P^\circ)}\right] = \alpha(T-T^\circ) - \kappa_T(P-P^\circ)\\ &\Rightarrow v = v(T^\circ,P^\circ)\frac{\exp[\alpha(T-T^\circ)]}{\exp[\kappa_T(P-P^\circ)]} \end{aligned} \tag{3}$$

$$\begin{aligned} g(T,P) = g(T,P^\circ) + \int_{P^0}^{P} v\,dP = g(T,P^\circ) + v(T^\circ,P^\circ)\exp[\alpha(T-T^\circ)]\int_{P^\circ}^{P}\exp[-\kappa_T(P-P^\circ)]dP\\ g(T,P) = g(T,P^\circ) + \frac{v(T^\circ,P^\circ)}{\kappa_T}\exp[\alpha(T-T^\circ)]\{1-\exp[-\kappa_T(P-P^\circ)]\} \end{aligned} \tag{4}$$

$$\begin{aligned} g(T,P^\circ) &= \Delta_f h^\circ(T) - Ts^\circ(T)\\ &= \Delta_f h^\circ(T^\circ) + \int_{T^0}^{T} C_p\,dT - Ts^\circ(T^\circ) - T\int_{T^0}^{T}\frac{C_p}{T}dT \end{aligned} \tag{5}$$

The heat capacity functions, $C_p(T)$ of gibbsite and boehmite have been fitted to experimental data according to Eq. (6):

$$C_p = a_0 + a_1T + a_2T^2 + a_3T^{-2} \tag{6}$$

so,

$$\begin{aligned} g(T,P^\circ) = \Delta_f h^\circ(T^\circ) + a_0(T-T^\circ) + \frac{a_1}{2}(T^2-T^{\circ 2})\\ + \frac{a_2}{3}(T^3-T^{\circ 3}) - a_3(T^{-1}-T^{\circ -1})\\ - T\left\{s^\circ(T^\circ) + a_0\ln\left(\frac{T}{T^\circ}\right) + a_1(T-T^\circ)\right.\\ \left. + \frac{a_2}{2}(T^2-T^{\circ 2}) - \frac{a_3}{2}(T^{-2}-T^{\circ -2})\right\} \end{aligned} \tag{7}$$

Table 6
Thermodynamic properties of the gibbsite and boehmite phases proposed in the present work, were ${}^{\circ}g(T,P) = g(T,P) - \sum_i H^{SER}_{298.15}$; i = Al(FCC), H_2(g), O_2(g).

Gibbsite ($Al_2O_3{\cdot}3H_2O$)	
Δh°_{f298} (J/mol)	−2594.3
s°_{298} (J/mol K)	139.4
$\Delta_f g^{\circ}_{298.15}$ (kJ/mol)	−2318.6
$C_p(T)$ (J/mol K)	$-37.714 + 0.91337T - 5.8953\times10^{-4}T^2 + 6.7386\times10^{3}T^{-2}$
${}^{\circ}g(T,P)$ (kJ/mol)	$-2.613921045\times10^{3} - 0.1434129694T - 4.56685\times10^{-4}T^2$
	$+9.8255\times10^{-8}T^3 - 3.3693T^{-1} + 3.7714\times10^{-2}T\ln(T)$
	$+1.56\times10^{6}\,e^{42\times10^{-6}T}[1-(1-2.067\times10^{-6})e^{-2.04\times10^{-11}P}]$
Boehmite ($Al_2O_3.H_2O$)	
Δh°_{f298} (J/mol)	−1981.1
s°_{298} (J/mol K)	96.86
$\Delta_f g^{\circ}_{298.16}$ (kJ/mol)	−1831.8
$C_p(T)$ (J/mol K)	$-24.038 + 0.56165T - 4.2275\times10^{-4}T^2 + 2.0153\times10^{3}T^{-2}$
${}^{\circ}g(T,P)$ (kJ/mol)	$-1.986155011\times10^{3} - 0.109201651T - 2.80825\times10^{-4}T^2$
	$+7.04583333\times10^{-8}T^3 - 1.00765T^{-1} + 2.4038\times10^{-2}T\ln(T)$
	$+2.052\times10^{8}\,e^{32.2\times10^{-6}T}[1-(1-9.55\times10^{-9})e^{-9.43\times10^{-14}P}]$

According to this, the expression of $g(T, P)$ function is the following one

$$\begin{aligned} g(T,P) &= \Delta_f h^{\circ}(T^{\circ}) + a_0(T-T^{\circ}) + \frac{a_1}{2}(T^2-T^{\circ 2}) \\ &+ \frac{a_2}{3}(T^3-T^{\circ 3}) - a_3(T^{-1}-T^{\circ -1}) \\ &- T\left\{ s^{\circ}(T^{\circ}) + a_0\ln\left(\frac{T}{T^{\circ}}\right) + a_1(T-T^{\circ}) \right. \\ &\left. + \frac{a_2}{2}(T^2-T^{\circ 2}) - \frac{a_3}{2}(T^{-2}-T^{\circ -2}) \right\} \\ &+ \frac{v(T^0,P^0)}{\kappa_T}\exp[\alpha(T-T^0)]\{1-\exp[-\kappa_T(P-P^{\circ})]\} \end{aligned} \tag{8}$$

so that, rearranging the terms of Eq. (8), the expression for the Gibbs free energy used in the present work is presented next,

$$\begin{aligned} g(T,P) &= b_0 + b_1T - a_0T^{\circ} - \frac{a_1}{2}T^{\circ 2} - \frac{a_2}{3}T^{\circ 3} + \frac{a_3}{T^{\circ}} \\ &+ \left[a_0(1-\ln T^{\circ}) + a_1T^{\circ} + \frac{a_2}{2}T^{\circ 2} - \frac{a_3}{2T^{\circ 2}}\right]T \\ &- \frac{a_1}{2}T^2 - \frac{a_2}{6}T^3 + \frac{a_3}{2T} + a_0T\ln \\ &T + \frac{v(T^{\circ},P^{\circ})}{\kappa_T}\exp[\alpha(T-T^{\circ})]\{1-\exp[-\kappa_T(P-P^{\circ})]\} \end{aligned} \tag{9}$$

where a_i (i = 0–3) and b_j (j = 0, 1) are the parameters to be calculated for gibbsite and boehmite.

The parameters needed for the description of the Gibbs free energy of gibbsite and boehmite (Eq. (9)) were optimized using the PARROT [72] module of the Thermo-Calc software. The different sets of experimental thermochemical and phase diagram data collected from literature were assigned different statistical weights during the optimization according to the accuracy reported in the original papers and the discussion in the following section. During the optimization, the heat capacity of gibbsite and boehmite were used first. Thereafter data of enthalpy, entropy and Gibbs free energy as well as phase diagram information were included.

Once the Gibbs free energy function were established for the phases, all equilibria were calculated using the module POLY-3 included in the Thermo-Calc databank system, version R [72].

4. Results and discussion

4.1. Assessment of the thermodynamic functions

Experimental measurements of $C_p(T)$ are scarce [37,39,48,61,65], however, the results obtained by the diverse author are in good agreement for gibbsite as well as for boehmite. In the present work, Eq. (6) was used to fit experimental data of $C_p(T)$, collected from bibliography. Table 6 shows the new calculated $C_p(T)$ functions, which showed a good agreement with the experimental data, as can be observed in Fig. 2.

On the contrary, an important dispersion was found in the experimental data of $\Delta_f h^{\circ}(T^{\circ})$, $s^{\circ}(T^{\circ})$ and $\Delta_f g^{\circ}(T^{\circ})$ for both gibbsite and boehmite phases. In Tables 2–4, the average values and standard deviation of thermodynamic functions at 298.15 K are exposed. In this work, molar Gibbs energy $g(T, P)$ has been calculated from Eq. (8), so that any variation in thermodynamic properties affects the values of $g(T, P)$ functions, and, as a consequence, the relative stability of the phases.

To analyze the effect of variations of thermodynamic properties on the relative stability of the phases, the upper and lower Gibbs free energy functions of gibbsite and boehmite have been evaluated, using the $C_p(T)$ functions calculated in the present work for each phase (Table 6). The functions $g^{upper}_{gibbsite}(T,P^{\circ})$, $g^{lower}_{gibbsite}(T,P^{\circ})$, $g^{upper}_{boehmite}(T,P^{\circ})$ and $g^{lower}_{boehmite}(T,P^{\circ})$ of the aluminium hydroxide phases were calculated using different values of $\Delta_f h^{\circ}(T^{\circ})$ and $s^{\circ}(T^{\circ})$, taken from the experimental data collected in Tables 3–5. Also the $g^{average}_{gibbsite}(T,P^{\circ})$ and $g^{average}_{boehmite}(T,P^{\circ})$ functions have been calculated from the average values of $\Delta_f h^{\circ}(T^{\circ})$ and $s^{\circ}(T^{\circ})$.

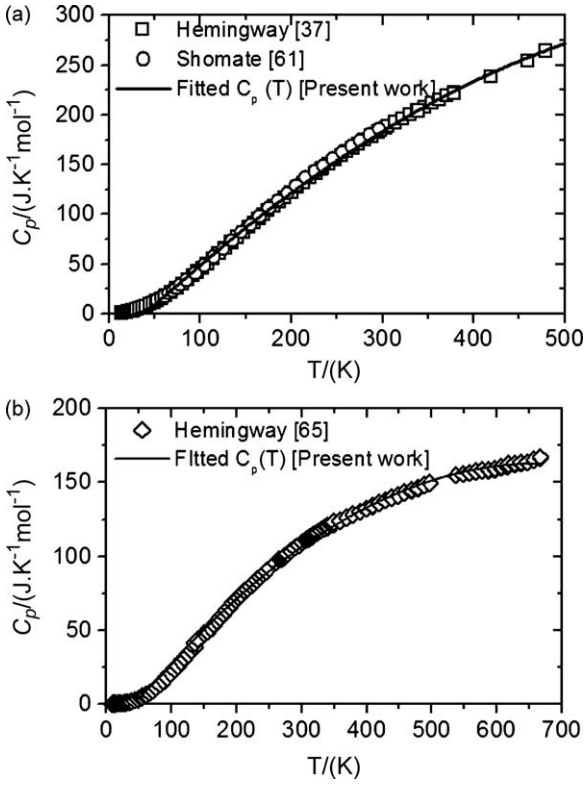

Fig. 2. (a) $C_p(T)$ function calculated in the present work (line) for gibbsite, compared with experimental data points (Shomate [61] (○) and Hemingway [37] (□)). (b) $C_p(T)$ function calculated in the present work (line) for boehmite, compared with experimental data points (Hemingway [65] (◇)).

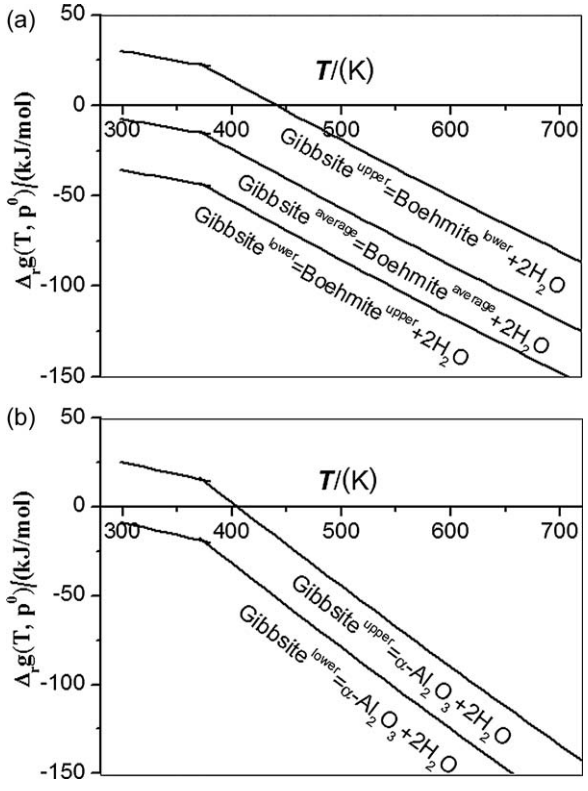

Fig. 3. $\Delta_r g(T, P^\circ)$ for different reactions using the lower and upper values for the Gibbs free energy functions of gibbsite and boehmite.

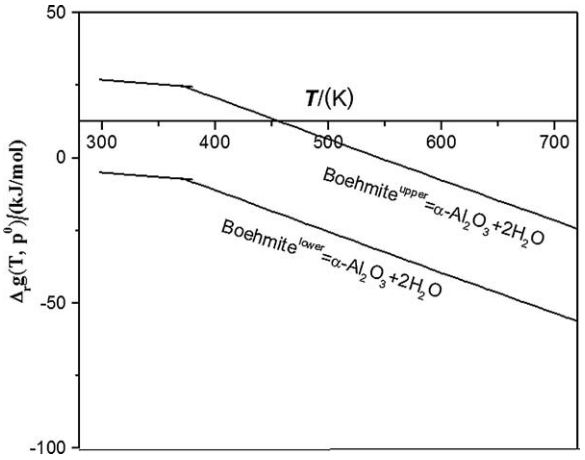

Fig. 4. $\Delta_r g(T, P^\circ)$ for different reactions using average values for the Gibbs free energy functions of gibbsite and boehmite.

The thermal stability of aluminium hydroxide phases at normal pressure conditions ($P^\circ = 1.03 \times 10^5$ Pa), can be studied in terms of $\Delta_r g$ in the reactions

$$\text{gibbsite}\,(Al_2O_3{\cdot}3H_2O) \rightarrow \text{boehmite}\,(Al_2O_3{\cdot}H_2O) + 2H_2O \quad (10)$$

$$\text{gibbsite}\,(Al_2O_3{\cdot}3H_2O) \rightarrow \alpha\text{-}Al_2O_3 + 3H_2O \quad (11)$$

$$\text{boehmite}(Al_2O_3{\cdot}H_2O) \rightarrow \alpha\text{-}Al_2O_3 + H_2O \quad (12)$$

where H_2O can be in liquid or gas state.

$\Delta_r g(T, P^\circ)$ of the reactions (10)–(12) are represented in Figs. 3 and 4. To simplify the discussion only the reaction with the stable form of H_2O at each temperature (H_2O liquid at $T < 373.15$ and H_2O gas at $T > 373.15$) has been represented. Taking into account that the reaction is possible for negative value for $\Delta_r g(T, P^\circ)$, the intersection of the $\Delta g_r(T, P^\circ)$ curve with the x-axes provides the temperature of decomposition of the aluminium hydroxide phase according to the corresponding reaction.

Fig. 3a and b shows the $\Delta g_r(T, P^\circ)$ of the reactions of decomposition of gibbsite into boehmite or corundum, according to reaction (10) or (11), respectively. Different results were obtained by combining the functions $g^{upper}_{gibbsite}(T, P^\circ)$, $g^{lower}_{gibbsite}(T, P^\circ)$, $g^{upper}_{boehmite}(T, P^\circ)$ and $g^{lower}_{boehmite}(T, P^\circ)$ as well as the $\Delta g_r(T, P^\circ)$ using $g^{average}_{gibbsite}(T, P^\circ)$ and $g^{average}_{boehmite}(T, P^\circ)$. According to Fig. 3a, gibbsite could be unstable at all temperatures with respect to boehmite or stable up to ~440 K. In particular, using the $g^{average}_{gibbsite}(T, P^\circ)$ and $g^{average}_{boehmite}(T, P^\circ)$ gibbsite would decompose to boehmite and liquid water even at ambient temperature. A similar behaviour can be deduced in the case of the decomposition of gibbsite in corundum; gibbsite could be unstable at all temperatures respect to α-Al_2O_3 or stable up to ~410 K.

A similar study has been done to analyze the stability of boehmite. Fig. 4 shows the $\Delta_r g(T, P^\circ)$ of the reactions of decomposition of boehmite following reaction (12). According this figure, boehmite could be unstable respect to α-Al_2O_3 at

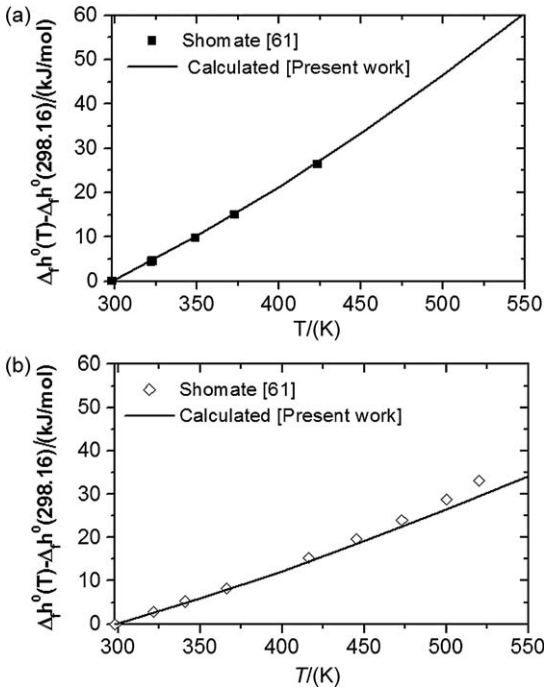

Fig. 5. Molar heat content ($\Delta_f h^\circ(T) - \Delta_f h^\circ$ (298.16)) calculated from thermodynamic functions provided in the present work for gibbsite (a) and boehmite (b) phases (line) compared with experimental data collected from bibliography (Shomate [61] (symbols)).

any temperatures or could be stable up to ~460 K depending on the value of $\Delta_f g^\circ(T^\circ)$ one uses.

All this discussion means that for gibbsite and boehmite, all intermediate combinations (relative stabilities) could be calculated by small modifications of the values of $\Delta_f h^\circ(T^\circ)$ and $s^\circ(T^\circ)$ within the experimental data/range.

Thermodynamic equilibrium calculations in the system Al_2O_3–H_2O have been shown to be extremely sensitive to very small changes in the values of the thermodynamic functions of the different aluminium hydroxide phases. In fact, not only the stability ranges, but also the relative stability of the phases are drastically modified by changing the values of the thermodynamic properties by 1%. The dispersion of the measured thermodynamic data of aluminium hydroxide phases collected in Tables 2–4, could be related with the different experimental methodologies and/or environmental conditions, as well as the presence of any impurity or solid solutions appearing in the studied materials or even the crystalline nature of the samples. The previous considerations mean that using only thermodynamic experimental data is not sufficient to safely describe the behaviour of the aluminium hydroxide phases. Moreover, it is important to note that the situation described by the Gibbs free energy functions calculated from the average values of $\Delta_f h^\circ(T^\circ)$ and $s^\circ(T^\circ)$ do not represent the actual observations. Typical temperatures reported for the decomposition of aluminium hydroxide phases (see Fig. 1) are clearly higher than those extracted from Figs. 3–5. In fact, there is no bibliographic data on decomposition of gibbsite at temperatures as low as 100 °C. The lower temperatures reported for decomposition of gibbsite into boehmite, as found in phase

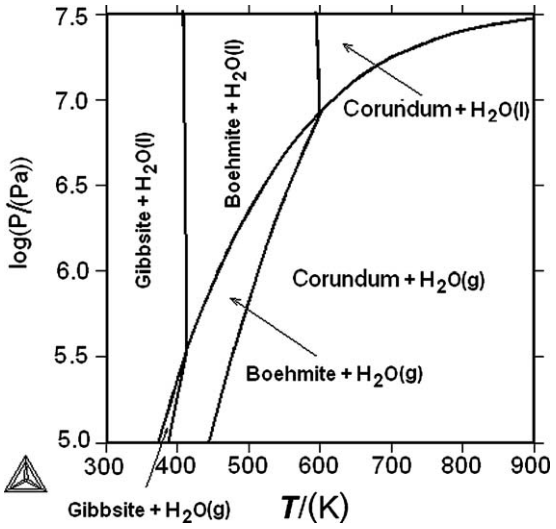

Fig. 6. *P–T* diagram for gibbsite and boehmite phases calculated from thermodynamic functions for gibbsite and boehmite phases provided in the present work.

equilibrium studies are 155 °C (428 K) [70] and 130 °C (403 K) [19]. The lowest temperature data reported for boehmite to α-Al_2O_3 decomposition was also found in phase equilibrium studies. Data from phase equilibrium diagram have been also taken into account in this work to optimize the $g(T, P)$ functions of the aluminium hydroxide phases.

The values of $g(T, P)$, $g^\circ(T^\circ)$, $\Delta_f h^\circ(T^\circ)$ and $s^\circ(T^\circ)$ and $C_p(T)$ assessed in the present work are shown in Table 6. C_p shows a good fit to the experimental data of Hemingway [48,65] and Shomate [61]. Resulting $\Delta_f h^\circ(T^\circ)$ of gibbsite (−2594.3 kJ/mol) differs by −0.47% from the average value, and $s^\circ(T^\circ)$ (139.4 J/mol K) differs by 0.66% from the average value being both calculated values within the experimental errors. $\Delta_f h^\circ(T^\circ)$ of boehmite (−1981.1 kJ/mol) differs by +0.281% of the average value. The calculated entropy $s^\circ(T^\circ)$ of boehmite was 96.86 J/mol K close to the value suggested by the most of authors and databases [10,36,61,67]. Experimental data of molar heat content ($\Delta_f h^\circ(T) - \Delta_f h^\circ$ (298.15)) measured by Shomate [61] can be compared with the values calculated from thermodynamic functions provided in the present work for both gibbsite and boehmite phases in Fig. 5. Thermodynamic calculation fits very well the experimental data of gibbsite. A good agreement was observed between thermodynamic calculations and experimental data for boehmite at lower temperature, but differences were observed at temperatures <450 K. However, according with the suggestion by Shomate [61], these may be uncertain by a few per cent as a function of increasing temperature.

4.2. Thermodynamic calculation of the P–T phase diagram of the system

The obtained $g(T, P)$ functions of the different phases allows one to calculate the *P–T* diagram shown in Fig. 6. The stability field of each phase is labelled, and the univariant curves forming the boundaries of these stability fields are thus transition curves along which the two neighbouring crystalline phases are in equilibrium with a fluid phase. The stability field

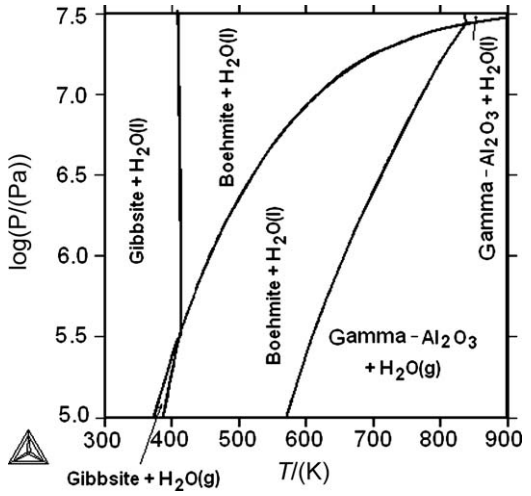

Fig. 7. *P–T* metastable relations for decomposition of gibbsite and boehmite phases into the γ-Al_2O_3 polymorph calculated from thermodynamic functions for gibbsite and boehmite provided in the present work.

of gibbsite is located in the low temperature range, boehmite in the intermediate range and the corundum stability field appears at higher temperatures. The univariant curve gibbsite ↔ boehmite + $2H_2O$ intersects the vaporization line of water at 413.2 K and 347,936 Pa (∼0.348 MPa) while the intersection of the univariant curve boehmite ↔ α-Al_2O_3 + H_2O with vaporization line takes place at 603.4 K and 8,794,274 Pa (∼8.79 MPa), that is, below the vaporization curve H_2O is in the liquid state and above the vaporization curve H_2O is in vapor. The *dP*/*dT* is positive for the univariant lines below the vaporization curve, and increases with temperature, as corresponding to a reaction giving rise to gaseous phase. The reaction boundary is curved and asymptotically approaches the temperature axis at low temperature, as is typical for a dehydration reaction. However, at pressures higher than that corresponding to vaporization curve, the fluid phase is a liquid, so that the compressibility is comparable to that of the solid. The reaction boundary and the *dP*/*dT* value put in evidence the difference in volume between the two solids. At normal pressure (100,000 Pa) decomposition temperatures of gibbsite and boehmite are 396.8 K and 438.6 K respectively. The experimental value on decomposition of gibbsite provided by Lauenbayen in hydrothermal conditions [70] is 15 K higher than that calculated in this study. The stability range reported for boehmite, between 428 K and 553 K [70], is within that calculated in the present work (413–603 K as a function of pressure). Stability field of gibbsite suggested by Ervin and Osborn [19] is 403 K at all pressure conditions, 10 K lower that the resulting in the present work in hydrothermal conditions. The stability range proposed by Ervin and Osborn [19] for boehmite at temperatures from 403 K (at normal pressure) up to 593 ± 15 K (at 13.8 MPa) is in line with the obtained in the present at low pressures, but discrepancies are observed at high pressures. However, it is important to note that Ervin and Osborn [19] suggest the existence of an inconsistent quaternary invariant point for coexistence of boehmite, diaspore, corundum and water at 613 ± 15 K (at 13.8 MPa), so that this data must be used carefully.

The shape of the stability field of gibbsite at pressure below the evaporation curve of the water puts in evidence that the temperature of decomposition of gibbsite significantly increases with increasing pressure. This can justify the higher temperature observed for decomposition of gibbsite in boehmite in samples with a large grain size or else highly crystallized [29,20].

It is important to note that all major studies on the hydration/dehydration behaviour of gibbsite and boehmite are done under dynamic conditions, far from equilibrium. This means that kinetic aspects are relevant so that other polymorphs of Al_2O_3 are formed in the samples. In order to analyze this topic, metastable decompositions of gibbsite and boehmite phases in the γ-Al_2O_3 metastable polymorph have been calculated. The thermodynamic functions of γ-Al_2O_3 have been taken from SSUB-3 database [69]. Fig. 7 shows *P–T* metastable relations for decomposition of gibbsite and boehmite phase into the γ-Al_2O_3 polymorph. In this figure, the univariant curve boehmite ↔ γ-Al_2O_3 + H_2O intersects the vaporization curve of water at 830 K and 27.47 MPa, while decomposition of boehmite would take place at 567.2 K at normal pressure. Typical temperatures reported for decomposition of boehmite in γ-Al_2O_3 polymorph are ∼720 K, which is in the range of the temperatures calculated in the present work. There is no thermodynamic data on the χ-Al_2O_3 polymorph, so the decomposition path form the gibbsite phase, according to the route A (Fig. 1) cannot be thermodynamically simulated.

5. Summary

In the present work, the *P–T* phase equilibrium diagram for the Al_2O_3–H_2O binary system at pressures up to 30 MPa has been thermodynamically assessed. A critical revision of the published experimental data of the system has been previously made. An optimized set of thermodynamic functions for the gibbsite and boehmite phases has been obtained from both experimental measurement of thermodynamic properties, and phase diagrams information. In the calculation, phases of the system have been treated as pure phases. The Gibbs free energy functions proposed in the present work are in good agreement with the thermodynamic experimental data and have allowed us to calculate a *P–T* diagram for the system, consistent with the experimental observations as well. The metastable *P–T* diagram for the system, considering the polymorph γ-Al_2O_3, has been also calculated, and the results are check out with the experimental observations in real materials.

Acknowledgements

The authors wish to acknowledge the financial support of the CICYT, Spain, Projects MAT 2004-04923-C02-01 and MAT 2007-65857.

References

[1] W.E. Dubbin, G. Sposito, M. Zavarin, X-ray absorption spectroscopic study of Cu-glyphosate adsorbed by microcrystalline gibbsite, Soil Sci. 165 (2000) 699–707.

[2] R. Weerasooriya, H.J. Tobschall, W. Seneviratne, A. Bandara, Transition state kinetics of Hg(II) adsorption at gibbsite–water interface, J. Hazard. Mater. 147 (3) (2007) 971–978.
[3] I.S. Park, M.S. Kwon, N. Kim, J.S. Lee, K.Y. Kang, J. Park, Rhodium nanoparticles entrapped in boehmite nanofibers: recyclable catalyst for arene hydrogenation under mild conditions, Chem. Commun. 45 (2005) 5667.
[4] Y. Kim, S.M. Lee, C.S. Park, S.I. Lee, M.Y. Lee, Substrate dependence on the optical properties of Al_2O_3 films grown by atomic layer deposition, Appl. Phys. Lett. 71 (1997) 3604.
[5] E.P. Gusev, M. Copel, E. Cartier, I.J.R. Baumvol, C. Krug, M.A. Gribelyuk, High-resolution depth profiling in ultrathin Al_2O_3 films on Si, Appl. Phys. Lett. 76 (2000) 176.
[6] G.C. Kennedy, Phase relations in the system Al_2O_3–H_2O at high temperatures and pressures, Am. J. Sci. 257 (1959) 563–573.
[7] S.C. Carniglia, Thermochemistry of the aluminas and aluminum trihalides, J. Am. Ceram. Soc. 66 (7) (1983) 495–500.
[8] L.M. Anovitz, D. Perkins, E.J. Essene, Metastability in near-surface rocks of minerals in the system $A1_2O_3$–SiO_2–H_2O, Clay Clay Miner. 39 (3) (1991) 225–233.
[9] T. Fockenberg, B. Wunder, K.D. Grevel, M. Burchard, The equilibrium diaspore–corundum at high pressures, Eur. J. Mineral. 8 (1996) 1293–1299.
[10] Outokumpu HSC Chemistry® for Windows v 5.11, Chemical Reaction and Equilibrium Software with Extensive Thermochemical Database.
[11] D.R. Lide (Ed.), CRC Handbook of Chemistry and Physics87th ed., 2006/2007, 6–120.
[12] M. Rivas, P. Pena, A.H. de Aza, D. Sheptyakov, X. Turrillas, On the decomposition of synthetic gibbsite studied by neutron thermodiffractometry, J. Am. Ceram. Soc. 89 (12) (2006) 3728–3733.
[13] H. Liu, J. Hu, J. Xu, Z. Liu, J. Shu, H.K. Mao, J. Chen, Phase transition and compression behavior of gibbsite under high-pressure, Phys. Chem. Miner. 31 (2004) 240–246.
[14] J.F. Beran, D. Grebille, P. Gregoire, D. Weigel, Thermal expansion of boehmite an anomaly near 560 K due to non-stoichiometric water, J. Phys. Chem. Solids 45 (1984) 147–150.
[15] B.J. Skinner, Thermal expansion. Handbook of physical constants, Geol. Soc. Am. Mem. 97 (1966) 75–96.
[16] F. Birch, Compressibility: elastic constants, in: Handbook of Physical Constants, Geol. Soc. Am. Mem. 97 (1966) 97–173.
[17] H.W. Van der Marel, H. Beutelspacher, Atlas of Infrared Spectroscopy of Clay Minerals and Their Admixtures, Elsevier, Amsterdam, 1976, p. 194.
[18] J.T. Huneke, R.E. Cramer, R. Alvarez, S.A. El-Swaify, Soil Sci. Soc. Am. J. 44 (1980) 131.
[19] G. Ervin, E.F. Osborn, The system Al_2O_3–H_2O, J. Geol. 59 (4) (1951) 381–394.
[20] M. Digne, P. Sautet, P. Raybaud, H. Toulhoat, E. Artacho, Structure and stability of aluminum hydroxides: a theoretical study, J. Phys. Chem. B 106 (2002) 5155–5162.
[21] R.S. Zhou, R.L. Snyder, Structures and transformation mechanisms of the η, γ and θ transition aluminas, Acta Crystallogr. 47 (1991) 617–630.
[22] I. Levin, D. Brandon, Metastable alumina polymorphs: crystal structures and transition sequences, J. Am. Ceram. Soc. 81 (8) (1998) 1995–2012.
[23] J. Rouquerol, F. Rouquerol, M. Ganteaume, Thermal decomposition of gibbsite under low pressures. I. Formation of the boehmitic phase, J. Catal. 36 (1975) 99–110.
[24] J. Rouquerol, F. Rouquerol, M. Ganteaume, Thermal decomposition of gibbsite under low pressures. II. Formation of microporous alumina, J. Catal. 57 (1979) 222–230.
[25] B.C. Lippens, J.H. De Boer, Study of phase transformations during calcination of aluminum hydroxides by selected area electron diffraction, Acta Crystallogr. 17 (1964) 1312.
[26] F. Paulik, J. Paulik, R. Naumann, K. Kijhnke, D. Petzold, Mechanism and kinetics of the dehydration of hydrargillites. Part I, Thermochim. Acta 64 (1983) 1–14.
[27] K.J.D. MacKenzie, J. Temuujin, K. Okada, Thermal decomposition of mechanically activated gibbsite, Thermochim. Acta 327 (1999) 103–108.
[28] H. Wang, B. Xu, P. Smith, M. Davies, L. DeSilva, C. Wingate, Kinetic modelling of gibbsite dehydration/amorphization in the temperature range 823–923 K, J. Phys. Chem. Solids 67 (12) (2006) 2567–2582.
[29] S.K. Mehta, A. Kalsotra, M. Murat, A new approach to phase transformations in gibbsite: the role of the crystallinity, Thermochim. Acta 205 (1992) 191–203.
[30] A. Sanoa, E. Ohtania, T. Kuboa, K. Funakoshib, In situ X-ray observation of decomposition of hydrous aluminum silicate $AlSiO_3OH$ and aluminum oxide hydroxide δ-AlOOH at high pressure and temperature, J. Phys. Chem. Solids 65 (2004) 1547–1554.
[31] M. Pourbaix, Atlas of Electrochemical Equilibria in Aqueous Solutions, Pergamon Press, 1966.
[32] D.D. Wagman, W.H. Evans, V.B. Parker, I. Halow, S.M. Bailey, R.H. Schumm, Selected values of chemical thermodynamic properties. U.S. Natl. Bur. Stand. Tech. (1968) Note 270-3.
[33] R.A. Robie, R. Waldbaum, Thermodynamic properties of minerals and related substances at 298.15 K (250 °C) and one atmosphere (1.013 bar) pressure and at higher temperatures, U.S. Geol. Surv. Bull. (1968) 1259.
[34] V.P. Glushko, Thermal Constants of Substances, vol. 5, VINITI, Moscow, 1971.
[35] L.V. Gurvich, I.V. Veyts, C.B. Alcock, Thermodynamic Properties of Individual Substances, vol. 1, Hemisphere Publishing Company, New York, 1989.
[36] D.D. MacDonald, P. Butler, The Thermodynamics of the aluminium–water system at elevated temperatures, Corros. Sci. 13 (1973) 259–274.
[37] B.S. Hemingway, R.A. Robie, J.R. Fisher, W.H. Wilson, Heat capacities of gibbsite, $Al(OH)_3$ between 13 and 480 K and magnesite, $MgCO_3$, between 13 and 380 K and their standard entropies at 289.15 K, and the heat capacities of calorimetry conference benzoic acid between 12 and 316 K, J. Res. U.S. Geol. Surv. 5 (6) (1977) 797–806.
[38] H.C. Helgeson, J.M. Delany, H.W. Nesbiti, D.K. Bird, Summary and critique of the thermodynamic properties of rock-forming minerals, Am. J. Sci. 278A (1978) 221–229.
[39] R.A. Robie, B.S. Hemingway, J.R. Fisher, Thermodynamic properties of minerals and related substances at 298.15 K and 1 bar (105 Pa) pressure and at high temperatures, USGS Bull. (1978) 1452.
[40] H.M. May, P.A. Helmice, M.L. Jackson, Gibbsite solubility and thermodynamic properties of hydroxy-aluminum ions in aqueous solution at 25 °C, Geochim. Cosmochim. Acta 43 (1979) 861–868.
[41] Y. Tardy, Kaolinite and smectite stability in weathering conditions, Estud. Geol. 38 (3–4) (1982) 295–312.
[42] O.A. Devina, M.E. Efimov, V.A. Medvedev, I.L. Khodakovsky, Geochem. Int. 20 (1983) 10.
[43] P.R. Bloom, R.M. Weaver, Effect of the removal of reactive surface material on the solubility of synthetic gibbsites, Clay Clay Miner. 30 (28) (1982) 1–286.
[44] F. Trolard, Y. Tardy, The stabilities of gibbsite, boehmite, aluminous goethites and aluminous hematites in bauxites, ferricretes and laterites as a function of water activity, temperature and particle size, Geochim. Cosmochim. Acta 51 (1987) 945–957.
[45] Y. Tardy, D. Nahon, Geochemistry of laterites. Stability of Al-goethite, Al-hematite and Fe^{3+}-kaolinite in bauxites and ferricretes. An approach to the mechanism of concretion formation, Am. J. Sci. 285 (1985) 865–903.
[46] F.J. Peryea, J.A. Kittrick, Relative solubilitv of corundum, gibbsite, boehmite and diaspore at standard state conditions, Clay Clay Miner. 36 (1988) 39l–396.
[47] Ch. Su, J.B. Harsh, Gibbs free energies of formation at 298 K for imogolite and gibbsite from solubility measurements, Geochim. Cosmochim. Acta 58 (6) (1994) 1667–1677.
[48] B.S. Hemingway, R.A. Robie, J.A. Kittrick, Revised values for the Gibbs free energy of formation of $[Al(OH)_4aq]$, diaspore, boehmite and bayerite at 298.15 K and 1 bar, the thermodynamic properties of kaolinite at 800 K and 1 bar, and the heats of solution of several gibbsite samples, Geochim. Cosmochim. Acta 42 (1978) 1533–1543.
[49] G.A. Parks, Free energy of formation and aqueous solubilities of aluminum hydroxides at 25 °C, Am. Mineral. 57 (1972) 1163–1189.
[50] V.C. Farmer, B.F.L. Smith, J.M. Tait, The stability, free energy and heat of formation of imogolite, Clay Miner. 14 (1979) 103–107.

[51] W.L. Bourcier, K.G. Knauss, K.J. Jackson, Aluminum hydrolysis constants to 250 °C from boehmite solubility measurements, Geochim. Cosmochim. Acta 51 (1993) 747–762.
[52] A.L. Reesmana, W.D. Keller, Aqueous solubility studies of high alumina and clay minerals, Am. Mineral. 53 (1968) 929–942.
[53] E.A. Zen, Gibbs free energy, enthalpy and entropy of ten rock-forming minerals. Calculations, discrepancies, implications, Am. Mineral. 57 (1972) 524–553.
[54] R. Barany, K.K. Kelley, Heats and free energies of formation of gibbsite, kaolinite, halloysite, and dickite, U.S. Bureau Mines Rept. Inv. 5825 (1961).
[55] P. Gross, J. Christie, C. Hayman, Heats of formation of gibbsite and light element double oxide, Fulmer Research Inst. Rept. 6, PG/JMN/R (1970).
[56] G.K. Johnson, I.R. Tasker, H.E. Flotow, P.A.G. O'Hare, W.S. Wise Thermodynamic studies of mordenite, dehydrated mordenite, and gibbsite, Am. Mineral. 77 (1992) 85–93.
[57] Q. Chen, W. Zeng, Calorimetric determination of the standard enthalpies of formation of gibbsite, Al(OH),(cr), and boehmite, AlOOH(cr), Geochim. Cosmochim. Acta 60 (1) (1996) 1–5.
[58] K. Yamada, T. Fukunaga, Y. Takahashi, T. Mukaibo, Heat of dehydration of hydrated alumina, Denki Kagaku 41 (4) (1973) 290–292.
[59] G. Verdes, R. Gout, S. Castet, Thermodynamic properties of the aluminate ion and of bayerite, boehmite, diaspore and gibbsite, Eur. J. Mineral. 4 (4) (1992) 767–792.
[60] J.A. Apps, J.M. Neil, C.-H. Jun, Thermochemical properties of gibbsite, boehmite, diaspore and the aluminate ion between 0 and 350 °C, Lawrence Berkeley Laboratory Rep. 21482 (1988).
[61] C.H. Shomate, O.A. Cook, Low temperature heat capacities and high temperature heat contents of $Al_2O_3{\cdot}3H_2O$ and $Al_2O_3{\cdot}H_2O$, J. Am. Chem. Soc. 68 (11) (1946) 2140–2142.
[62] G.B. Naumov, B. Ryzhenko, I.L. Kodakovsky, Handbook of Thermodynamic Data, Moscou Atomizdat, 1971.
[63] K.K. Kelley, Bulletin 584, U.S. Bureau of Mines, 1960.
[64] V.A. Pokrovskii, H.C. Helgeson, Thermodynamic properties of aqueous species and the solubilities of minerals at high pressures and temperatures: the system Al_2O_3–H_2O–NaCl, Am. J. Sci. 295 (1995) 1255–1342.
[65] B.S. Hemingway, R.A. Robie, J.A. Apps, Revised values of the thermodynamic properties of boehmite, AlO(OH), and related species and phases in the system Al–H–O, Am. Mineral. 76 (1991) 445–457.
[66] D. Perkins, E.J. Essene, E.F. Westrum, V.J. Wall, New thermodynamic data for diaspore and their application to the system Al_2O_3–SiO_2–H_2O, Am. Mineral. 64 (1979) 1080–1090.
[67] N.B.S. Technical Note 270-3 (1968).
[68] C.E. Wicks, Bulletin 605, U.S. Bureau of Mines, 1963.
[69] SSUB3, SGTE Substance Database (Version 3.1 2001/2002), SGTE, Scientific Group Thermodata Europ.
[70] A.W. Laubengayer, R.S. Weisz, A hydrothermal study in the system alumina-water, Am. Chem. Soc. J. 65 (1943) 247–250.
[71] F. Dachille, P. Gigl, Two high-pressure $Al(OH)_3$ phases and contributions to the Al–Al_2O_3–H_2O system, High Temp.-High Press. 15 (1983) 657–675.
[72] Thermo-Calc Software, version R, Thermo-Calc Software AB, www.thermocalc.com, Copyright (1995, 2003) Foundation for Computational Thermodynamics, Stockholm, Sweden.